Journal of Alloys and Compounds 776 (2019) 297–305

Contents lists available at ScienceDirect

Journal of Alloys and Compounds

journal homepage: http://www.elsevier.com/locate/jalcom

Effect of solid fraction on microstructures and mechanical properties of a Mg-Al-La-Ca alloy processed by rheocasting

Sérgio L.T. Bartex [a, *], Carlos A. dos Santos [b], Vinicius K. de Barcellos [a], Lírio Schaeffer [c]

[a] Foundry Laboratory, Department of Metallurgy, Federal University of Rio Grande do Sul - UFRGS, Bento Gonçalves Av., 9500, ZIP Code 91501-970, Porto Alegre, RS, Brazil
[b] Materials Laboratory, School of Technology, Pontifical Catholic University of Rio Grande do Sul - PUCRS, Av. Ipiranga, 6681, 90619-900, Porto Alegre, RS, Brazil
[c] Metal Forming Laboratory, Department of Metallurgy, Federal University of Rio Grande do Sul - UFRGS, Bento Gonçalves Av., 9500, ZIP Code 91501-970, Porto Alegre, RS, Brazil

ARTICLE INFO

Article history:
Received 5 July 2018
Received in revised form
8 October 2018
Accepted 23 October 2018
Available online 24 October 2018

Keywords:
Magnesium alloy
Rheocasting
Solid fraction
Microstructure
Mechanical properties
La-Ca

ABSTRACT

Morphological evolution of microstructures and tensile properties in Mg-Al alloy containing La and Ca (Mg-6Al-3La-1Ca) processed by rheocasting with different solid fractions (fs) were investigated at this paper. An apparatus for semisolid metal alloy processing was used to melt and to obtain the rheocast material. Isothermal mechanical stirring experiments were carried out with fs = 0.30, 0.49 and 0.61 at 950 rpm for 10 min. A conventional casting (no stirring) was also obtained for comparisons. Results showed that microstructure in conventional casting is composed by α-Mg dendritic matrix and $Al_{11}La_3$, $(Al,Mg)_2Ca$ and Mg_2Ca compounds. Non-dendritic and globular microstructures were observed in the rheocasting. For fs = 0.30 the acicular $Al_{11}La_3$ phase precipitated at globule boundaries, while for the fs = 0.49 and fs = 0.61 the acicular phase precipitated both inside and at globule boundaries. The ideal rheocasting condition was achieved fs = 0.30 due to the improvement of 76% for the ultimate tensile strength (UTS) and 80% in the strain to fracture when compared to the conventional casting. Fracture surface analysis pointed to a mixed ductile-brittle fracture mode containing dimples and quasi-cleavage facets for the lowest solid fraction (fs = 0.3), and a fully brittle fracture mode consisting exclusively of cleavage planes for the highest solid fraction (fs = 0.61).

1. Introduction

Lightweight design has become a tendency in automotive, aircraft and aerospace industry for energy saving [1]. Magnesium-based alloy is one of promising alternative materials due to its low density, high specific strength, good fusibility and good recyclability [2]. However, Mg alloys have both inferior mechanical properties and heat resistant quality when compared with aluminum-based cast alloys, and this fact restricts their wide application. In order to overcome mechanical properties limitations, alloying elements are added to magnesium, and the most important is aluminum. However, the β-phase ($Mg_{17}Al_{12}$) formation has been related as responsible to poor mechanical resistance of magnesium alloys at high temperatures [3,4].

To solve this problem, Rare-Earths (RE) additions are used to prevent or to reduce the β-phase formation because the RE elements can combine with aluminum developing stable intermetallics instead of the poor β-phase $Mg_{17}Al_{12}$. This contributes to improve both creep and mechanical properties in general [5]. Addition of high content of RE and AE permits to magnesium alloys excellent properties, but it is difficult for them to be widely used because of their high cost [1,6]. Nevertheless, researches [3–7] on texture modification of Mg alloys are focused on microalloying with specific elements in which Rare Earth (RE) and Alkaline Earth (AE) elements have been used together, for example lanthanum (La) and calcium (Ca).

On the other hand, traditional manufacturing process including sand and permanent casting which are generally used to produce components tend to induce defects such as porosity, segregation and very coarse micro compounds to the casting products. A good way to reduce these defects is the semisolid rheocasting technology [8]. In this process, liquid metal is transformed into semisolid

* Corresponding author.
E-mail addresses: bartex@ufrgs.br (S.L.T. Bartex), vinicius.karlinski@ufrgs.br (V.K. de Barcellos).

https://doi.org/10.1016/j.jallcom.2018.10.292
0925-8388/

slurries. The slurries can be formed at different solid fractions. However, the ability to rapidly apply the process using existing machines requires the production of slurries having low solid fractions in the range of 10–50% [9].

Rheocasting process to be efficiently applied needs an appreciable melting range and several process controls to improve the quality of the slurry. Homogeneous and globular microstructure is aimed, and to achieve these requirements it is important to understand the formation mechanism of globular structure during rheocasting processes [10].

The most popular theory about globular structure formation is to apply a physical field in a semisolid metal, and the dendrite arms will be fragmented becoming its morphology globular by Ostwald ripening phenomena [11–13]. Many methods to prepare non-dendritic semisolid slurries have been proposed such as twin screw shearing [14], gas bubble stirring [15], ultra-sonic vibration [16], electro-magnetic stirring [8], and mechanical stirring [17]. Mechanical stirring is one of most common way used to produce rheocasting products. However, parameters like stirring temperature, solid fraction and stirring velocity could have a strong influence on quality of ingots. Many researches [11,12,18] have investigated the influence of low stirring velocity (less than 500 rpm) in globular formation, but they have no enough information about stirring velocities higher than 500 rpm.

Despite the numerous works reported in the literature, the knowledge about the morphological microstructure evolution and mechanical responses in Mg-Al-La-Ca alloys subjected to rheocasting processing is unclear. This work intends to understand the solidification sequence and the effect of solid fraction in the microstructural features and tensile properties of a Mg-6wt%Al-3wt%La-1wt%Ca alloy processed by isothermal mechanical stirring in different rheocasting conditions.

2. Experimental procedure

The analyses were performed using magnesium ingots produced by a Brazilian company, whose chemical composition determined by ICP-OES: Inductively Coupled Plasma Optical Emission Spectroscopy is presented in Table 1. The values represent the average results of five measurements.

A resistance-type electric closed furnace with a protective gas atmosphere (commercial argon gas, 99.9% purity) was designed to prevent any reaction between oxygen and the magnesium molten in order to avoid ignition [2]. The ingots with 1 kg mass were melted in the furnace using an ASTM A420 stainless steel crucible (118 mm-diameter and 50 mm-height). A steel mechanical stirrer coupled in an electric motor was used for the mechanical stirring experiments. A schematic representation of the apparatus is presented in Fig. 1a. The temperature data were acquired during solidification by two K-type thermocouples (1.6 mm diameter, AISI/SAE 446 chromium-steel) accurately positioned one at the crucible center and other in the crucible wall at 4 mm distance from the metal/mold interface. Both thermocouples were located 15 mm from the bottom of the crucible. In all experiments, the argon flux with 5 L/minute was maintained during heating, melting and cooling of the alloy.

In order to verify the melting range of the alloy (interval between *Liquidus* and *Solidus temperatures*), a slow cooling casting condition, labeled Experiment 1, was performed. The slow cooling condition, as close as possible to the thermodynamic equilibrium, was obtained by powering-off the furnace when the alloy reached the desired temperature (740 °C). The cooling curves were used to determine the solidification parameters by the Computer-Aided Cooling Curve Thermal Analysis (CA-CCTA) technique [19]. A Differential Scanning Calorimetry (DSC) analysis was also utilized to confirming the melting range. The rheocast conditions, labeled as

Table 1
Chemical composition of the magnesium alloy (wt. %).

Elements								
Mg	Al	Zn	Mn	Fe	Cu	Ni	Ca	La
Balance	5.9	0.03	0.3	0.0058	0.0024	0.0012	0.988	2.77

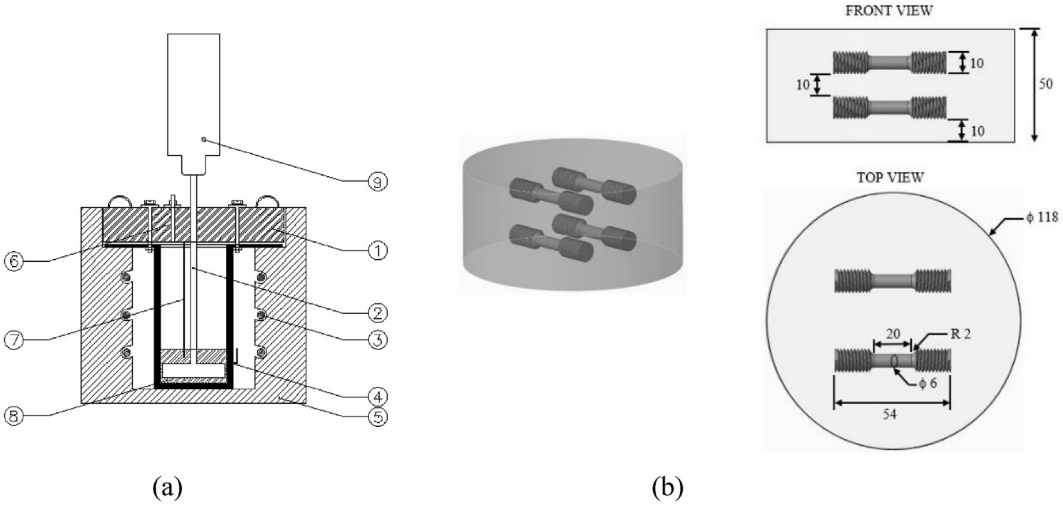

Fig. 1. (a) Schematic representation of the experimental arrangement: *1*- insulated cover system; *2*- mechanical stirrer; *3*- electrical resistances; *4*- crucible wall thermocouple; *5*- thermal insulation; *6*- argon inlet; *7*- internal thermocouple; *8*- crucible; *9*- stirrer. (b) Samples extracted for metallography and tensile testing (dimensions in mm).

Experiments 2, 3 and 4, were performed as the following experimental sequence: the alloy was completely melted at 650 °C, after that, the temperature was decreased to the stirring temperatures, as given: 605 °C, 595 °C and 585 °C. These temperatures were chosen to reduce 10 °C, 20 °C and 30 °C, respectively, below the *Liquidus* temperature to analyze the effect of different solid fractions in the mechanical stirring process. A cooling rate of 10 °C/min was applied between melting and stirring temperatures. To mechanical stirring stage was used 950 rpm, 10 min stirring time and isothermal condition to all experiments. After stirring, the crucible containing the semisolid alloy was removed from the furnace and cooled in a water bath at 25 °C. In the last condition, labeled Experiment 5, conventional casting was analyzed using the same thermal process parameters used in Experiment 2, but the mechanical stirring stage was omitted. This experiment was carried out to compare the stirred and non-stirred ingots. Table 2 summarizes the experimental conditions.

In order to analyze the microstructures and mechanical properties, four samples were extracted from each ingot as shown in Fig. 1b. The tensile specimens were machined according to ASTM B557-06 [20]. The average values of yield strength (YTS), ultimate tensile strength (UTS) and strain to fracture (ε) were expressed to each condition. The microstructures were analyzed in cross sections of the specimens after tensile testing by optical microscope (OM), scanning electron microscope (SEM) and energy dispersive spectroscopy (EDS) using mapping mode. For optical microscope analyzes the samples were etched by a Nital 3% solution (3 ml HNO_3 + 97 ml ethanol). The globule area was measured by Image J software and equivalent diameter (De) was calculated. The equivalent diameter can be defined as the diameter of a circle having the same area as the globule. Then the shape factor (f) was calculated by the follow equation:

$$f = \frac{4.\pi.A}{p^2} \quad (1)$$

where A and p are, respectively, area and perimeter of primary solid particle [18].

3. Results and discussion

Fig. 2a presents the results of the thermal analysis during solidification with slow cooling condition (Experiment 1) using the CA-CCTA method, showing the cooling curve and the first derivative. The cooling rate was 0.03 °C/s for Experiment 1. The first reaction is related to the α-Mg matrix formation that occurs at 615 °C. The second reaction at 605 °C is associated to the $Al_{11}La_3$ phase, and the third and fourth reactions, that occur at 526 °C and 512 °C, respectively, are related to the α-Mg + Al_2Ca and α-Mg + Mg_2Ca eutectic formations [4,5,21]. The last transformation at 401 °C is related to the solid-state transformation that occurs below the *Solidus* temperature, and is probably due to the Al-Ca compounds formation.

The DSC result presented in Fig. 2b shows the same tendency, with exothermic peaks at 614 °C, 604 °C, 526 °C and 511 °C. The maximum temperature difference between the CA-CCTA and the DSC analyses was at 1 °C, indicating the reliability of the results.

Comparing the thermal analysis with literature data the solidification path that can be summarized in the following sequence: L → α-Mg + L1 (615 °C), L1 → $Al_{11}La_3$ + L2 (605 °C), L2 → (Mg,Al_2)Ca + L3 (526 °C), L3 → Mg_2Ca + L4 (512 °C). The *Liquidus* and *Solidus* temperatures were determined at 614 °C and 511 °C, respectively. These results pointed a large melting range, ideal to semisolid processing [18]. The identified phases and the transformation temperatures agree with results reported in the literature [1,4,5]. According to Liang et al. [22], the addition of Ca in Mg-Al alloys suppresses the β-$Mg_{17}Al_{17}$ phase, and a eutectic mixture composed of α-Mg and Al_2Ca is formed at 614 °C. They suggested that when the Ca/Al ratio is greater than 0.8, the Mg_2Ca phase is present in a eutectic structured formed at 510 °C. In the present work, the eutectic α-Mg + Mg_2Ca was observed with a Ca/Al ratio equal 0.167, and it permits to concluded that the addition of lanthanum can induce this reaction. However, further

Table 2
Experimental conditions.

Experiment	Cooling Condition	Casting Condition	Stirring Temperature (°C)	Stirring Time (min.)
1	Air, slow cooling	Conventional	–	–
2	Water, fast cooling	Rheocasting	605	10
3	Water, fast cooling	Rheocasting	595	10
4	Water, fast cooling	Rheocasting	585	10
5	Water, fast cooling	Conventional	–	–

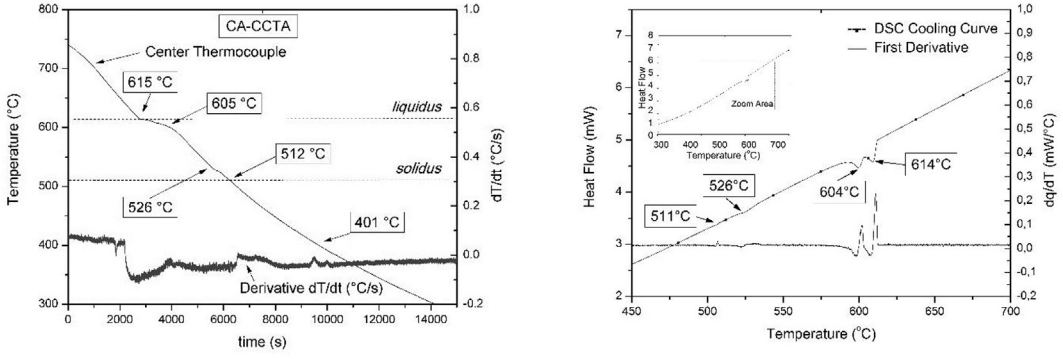

Fig. 2. Thermal analysis results of the: (a) CA-CCTA and (b) DSC methods in the slow cooling condition (Experiment 1).

investigations are required in this question.

The microstructures of the slow cooling casting (Experiment 1) are presented in Fig. 3a. It is possible to identify the α-Mg matrix (dark areas) with a dendritic morphology, the precipitate $Al_{11}La_3$ (white area) with an acicular or needle-shaped morphology, and the two eutectic structures α-Mg + Al_2Ca with a networked structure and α-Mg + Mg_2Ca with a Chinese script-like morphology. For the rheocast condition (Experiment 2), non-dendritic and globular microstructure was observed, as seen in Fig. 3b. The identifications were based on the analyses of the EDS spectra (Fig. 3c) and the characteristic morphologies of the structures reported in the literature. The precipitate and the eutectic structures are both predominantly formed in the interdendritic regions. In the case of the $Al_{11}La_3$, the needles can also be formed into the dendrites and growth across the interdendritic regions [21]. When analyzing the microstructures in ternary and quaternary Mg-based alloy systems with Ca and La additions, the results agree with those reported in the literature [1,21]. According to Zhang et al. [1], when the Zn content is low in the Mg-Al-RE (Rare Earths) alloys, the predominant formed structures are the Al-RE and Al-Ca, with the $Al_{11}La_3$ phase being typically observed. Similar results were reported by Han et al. [23] in Mg-Al-Ca alloys with different Ca contents. It was confirmed that the Al_2Ca phase presents a hexagonal structure, consisting in a networked structure with the α-Mg, preferentially in the grain or dendrites boundaries. Recently, Liu et al. [24] have investigated the Al_2Ca phase in a Mg-Al-Ca-Mn alloy using the TEM analysis, and they observed two kinds of morphologies, a plate-shaped and a cone-shaped with respect to the α-Mg matrix.

Fig. 4 shows a SEM micrograph and the elemental map obtained by the EDS for the Experiment 2 (rheocasting condition at 605 °C). The EDS image (Fig. 4b) confirms that magnesium is predominantly present in the matrix, while aluminum (Fig. 4c), calcium (Fig. 4d) and lanthanum (Fig. 4e) are observed in the interglobular regions. Aluminum is distributed in both the network structure (Fig. 4c) and the acicular phase (Fig. 4f), in association with calcium and lanthanum, respectively. The presence of calcium is associated to the formation of the structure with a Chinese-script morphology and the refined network structure [25]. Comparing Figs. 3 and 4a, the matrix changed from dendritic to a globular morphology. Also, can be noted that compounds are distributed on the globular boundaries, and globules center are composed mainly by magnesium with any other elements in the solid solution.

In order to determine the solid fraction (f_s), the temperatures obtained in the DTA results and the Scheil formulation (Equation (2)) were utilized assuming local equilibrium at the liquid/solid interface, complete mixing of the liquid by stirring and considering no diffusion through the solid, and expressed as:

$$fs = 1 - \left(\frac{T_M - T}{T_M - T_L}\right)^{\left(\frac{1}{k-1}\right)} \quad (2)$$

where k is the equilibrium partition coefficient, T_M is the melting temperature of the pure solvent, and T_L is the *Liquidus* temperature of the alloy with initial concentration C_0. In this work, the following values were considered: $T_M = 650\,°C$, $T_L = 615\,°C$ and $k = 0.37$. As results of Equation (2), the solid fractions were calculated as 0.30 for the isotherm temperature at 605 °C, 0.49 at 595 °C and 0.61 at 585 °C.

Fig. 5 shows the optical micrographs of the alloy in conventional casting and rheocasting conditions. Fig. 5d shows the microstructure of the Experiment 5 (fast cooling), while the others images present the microstructures of the Experiments 2 to 4 (rheocasting).

It is possible to observe the morphological change in the matrix from dendritic to globular, when compared Fig. 5d to other. For the lowest solid fraction (fs = 0.30), the acicular phase ($Al_{11}La_3$) was not found inside the globules in Fig. 5e. This fact is related to the initial formation temperature of the $Al_{11}La_3$ phase that occurs at 605 °C. The α-Mg matrix begins the natural solidification path at 615 °C with a dendritic morphology. During this process, due to solubility difference between solid and liquid, the other alloy elements are segregated to the interdendritic reminiscent liquid. The solidification continues until 605 °C and, at this temperature, the $Al_{11}La_3$ phase is still not precipitated. At this moment, the mechanical stirring starts, and the α-Mg dendrites are broken and become morphologically globular due to the Ostwald Ripening phenomena [8]. The final microstructure is composed by globular α-Mg matrix surrounded by acicular phase ($Al_{11}La_3$) and precipitated eutectics (Al_2Ca and Mg_2Ca) in the globular boundaries.

However, for higher solid fractions (fs = 0.49 and fs = 0.61) can be observed in Fig. 5f and g the acicular phases present both inside and at globule boundaries. In these cases, the first solidification step is the same presented later. However, the stirring temperatures on Experiment 3 (595 °C) and 4 (585 °C) are less than 605 °C. The consequence is the precipitation of the acicular phase ($Al_{11}La_3$) inside of the globules. At these temperatures, the mechanical stirring begins and breaks the dendritic arms. As consequence, the primary α-Mg presents acicular phase inside and at globule boundaries, as indicated in the images by arrows. The $Al_{11}La_3$ phase

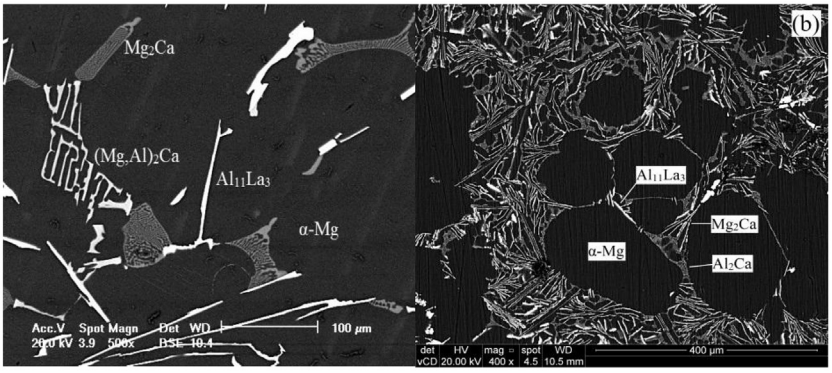

EDS results (At. %)

Mg	Al	La	Ca	Phase
100	-	-	-	α – Mg
66	27	7	-	$Al_{11}La_3$
67	20	-	13	$(Mg,Al)_2Ca$
72	8	-	20	Mg_2Ca
93	5	-	2	Mg-Al-Ca

(a) (b) (c)

Fig. 3. SEM images: (a) Experiment 1 - slow cooling casting condition, (b) Experiment 2 - rheocasting, and (c) EDS results for both conditions.

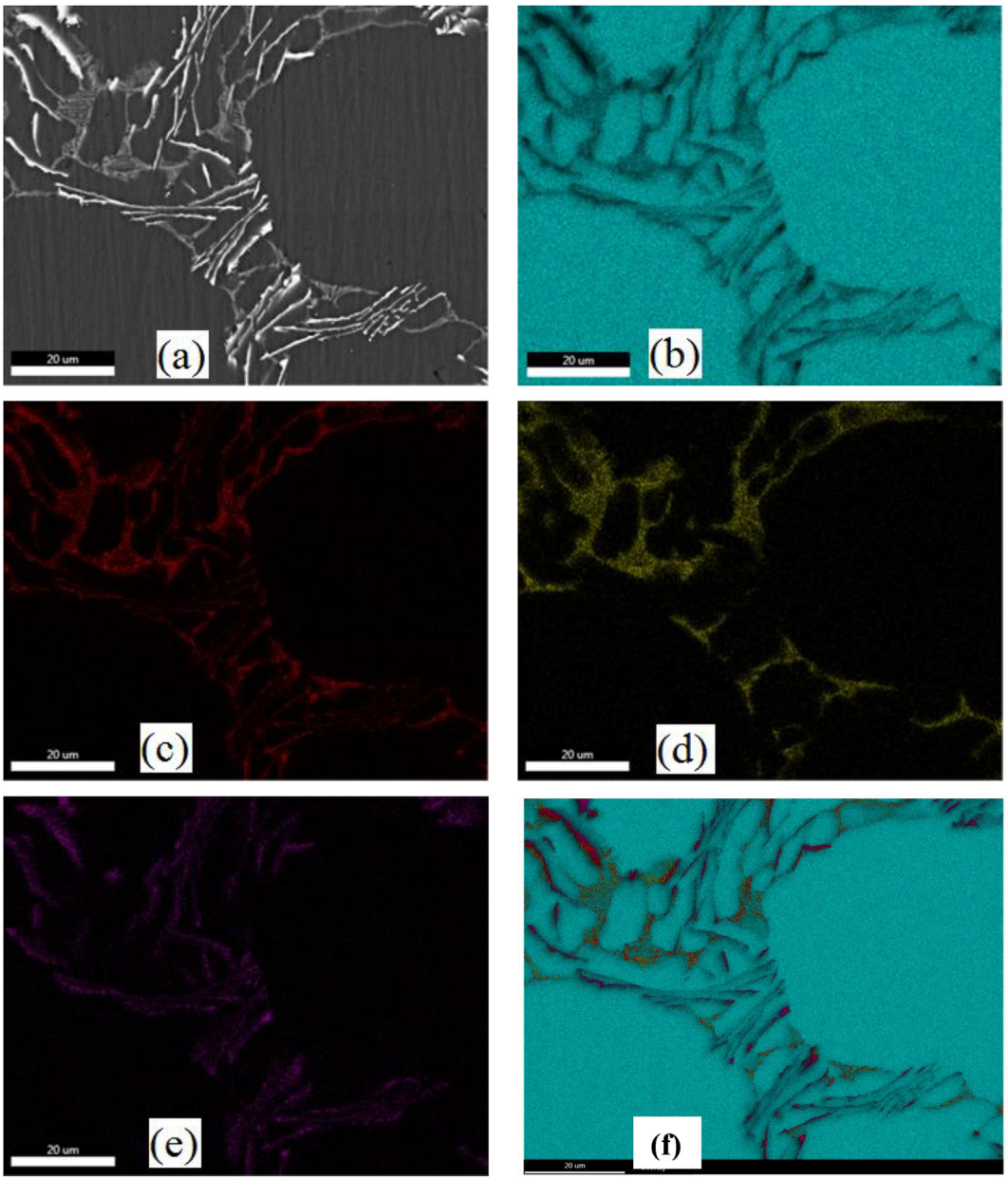

Fig. 4. (a) SEM image and elemental maps for: (b) magnesium; (c) aluminum; (d) calcium; (e) lanthanum; and (f) all elements of the rheocasting condition at 605 °C.

has higher size in Fig. 5f and g when compared with Fig. 5e.

Using an image analysis software, the equivalent diameter (De) and shape factor (f) were determined in function of the rheocasting condition, as shown in Fig. 6a. The equivalent diameter is proportional to the solid fraction, so small solid fraction values means small and refined globules. These occurs because at small solid fraction is easy to break the dendritic structure resulting in small solid particles along to liquid, and the morphology changes from dendritic to spherical shape to minimize the surface energy by the Ostwald ripening process [26]. However, when the solid fraction increases the size of dendrites also increases, and the equivalent diameter becomes irregular and coarse. The average and standard deviation values confirm this tendency.

On the other hand, the shape factor has an inverse behavior in relation to the solid fraction. For higher solid fraction, the dendritic shear resistance increases and become more difficult the globularization, and the solid particles will be coarse, irregular and the shape factor is about 0.5. As the solid fraction decreases, the dendrites present lower shear resistance and the solid structures tend to present the shape factor about 0.8. Standard deviation on shape factor to the condition with fs = 0.61 is higher than other conditions (fs = 0.49 and fs = 0.30), showing more irregular globules with the increasing in the solid fraction.

Fig. 6b shows the tensile responses of the rheocasting conditions. The solid fraction and the tensile strength have an inverse relationship. This behavior can be attributed to the decreasing of the equivalent diameter as shown in Fig. 6a. The equivalent diameter decreases with smaller solid fractions and this creates more globule boundaries that difficult the crack propagation. Also, when the acicular $Al_{11}La_3$ phase and the Al_2Ca and Mg_2Ca eutectics precipitate in the interglobular region, they create a barrier to dislocations movement [27].

In the same way, the strain to fracture values have an inverse relationship with solid fraction. Analyzing the microstructures in

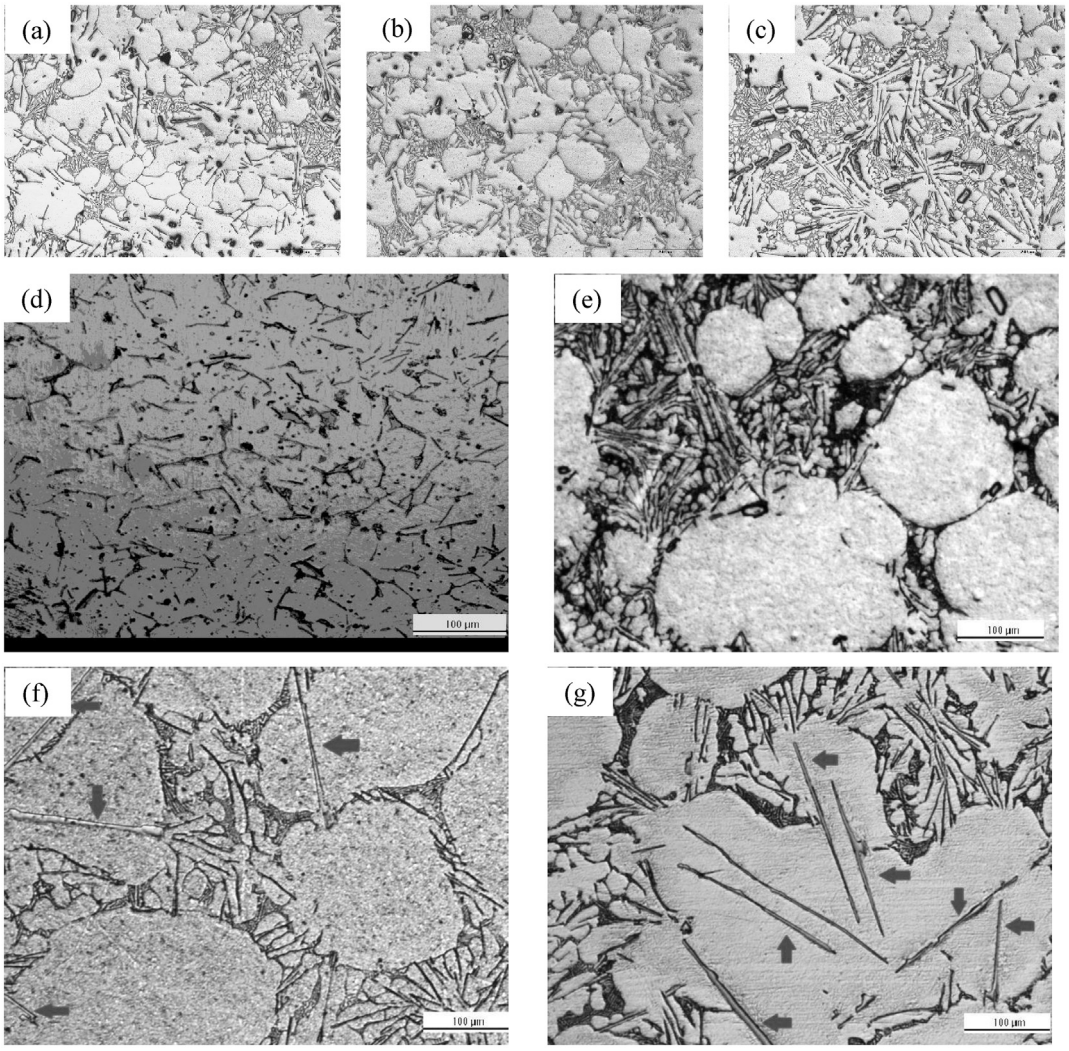

Fig. 5. Optical micrographs in low magnification: (a) $f_S = 0.30$ (Exp.2); (b) stirred, $f_S = 0.49$ (Exp.3); (c) stirred, $f_S = 0.61$ (Exp.4). High magnification: (d) fast cooling casting, no stirred (Exp.5); (e) rheocasting, stirred, $f_S = 0.30$ (Exp.2); (f) stirred, $f_S = 0.49$ (Exp.3); (g) stirred, $f_S = 0.61$ (Exp.4). Arrows pointing location of acicular phase.

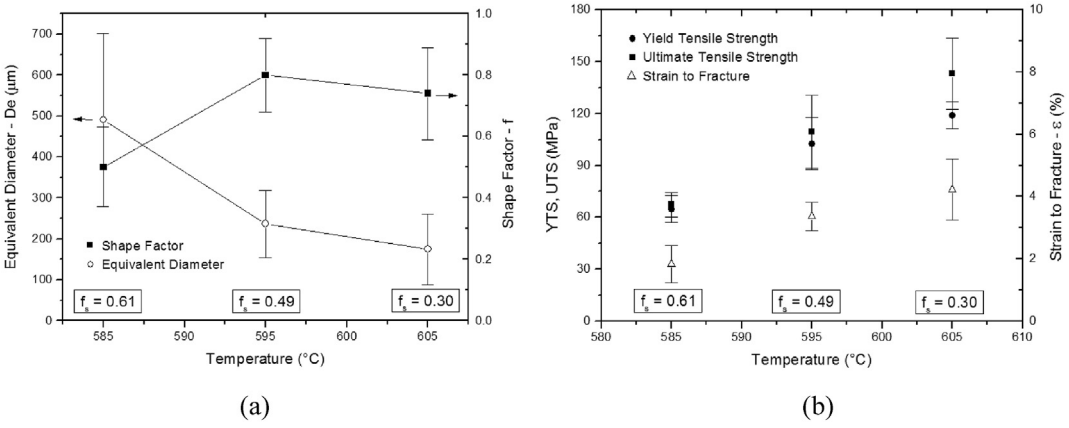

Fig. 6. (a) Equivalent diameter and shape factor in function of the temperature, (b) tensile responses in function of the temperature and the solid fraction of the rheocasting conditions.

Fig. 5 and deformations in Fig. 6b, it can be attributed the presence of acicular phase inside of globules as responsible to reduced plastic deformation in α-Mg matrix. In addition, it was observed higher deformation for $fs = 0.30$ due to the absence of acicular phase precipitated inside of the globules.

Comparing Fig. 6a and b, it can be seem that the equivalent diameter has an inverse relationship with YTS and UTS. The obtained values of ultimate tensile strength and strain to fracture for

the Experiment 4 (fs = 0.3) are similar to those reported by Zhang et al. [1] with Mg-Zn-Al-La-Ca alloys. For Experiment 5 the YTS, UTS and strain to fracture values were, respectively, 75.69 ± 11,01 MPa, 81.20 ± 8.30 MPa and 2.34 ± 0.14.

Fig. 7 shows images of the fracture surfaces obtained by SEM of the samples after tensile testing in the rheocasting and conventional casting conditions. For the lowest and highest solid fractions (fs = 0.30 and fs = 0.61), two images with different magnifications are presented in order to permit better interpretations. In an overall view, the rheocasting samples (Fig. 7a–e) showed a mixed ductile-brittle fracture mode with the presence of cleavage facets, quasi-cleavage planes and irregular dimples in the α-magnesium matrix [28], while the conventional casting sample (Fig. 7f) presented a fully brittle fracture aspect with cleavage planes, river patterns and micro-cracks. This confirms that the rheocasting samples presented a more ductile fracture mode when compared to the conventional casting (Fig. 7e), and this aspect have reflected in higher strain to fracture for rheocasting samples (Fig. 6b).

In the lowest solid fraction (fs = 0.30 at 605 °C), the amount of cleavage planes is almost insignificant, the presence of quasi-cleavage and dimples is predominant (Fig. 7a), and the crack propagation followed the transgranular mode.

The surface fracture of the rheocasting sample with fs = 0.49 (at 595 °C) shows that fracture occurred preferably at the globule boundaries (Fig. 7e), with small amount of dimples and cleavage planes, configuring an interglobular crack propagation mode.

When the solid fraction was increased to 0.61 (at 585 °C), the viscosity of the metal also increased, and the surface fracture indicates the lack of liquid penetration in some regions, as well as the presence of a dendritic structure in material [29–31]. The fracture path was preferential in these regions. This indicates that solid fraction higher than 0.5 is not adequate to obtain globular structures [32,33].

For the conventional casting (Fig. 7f), the surface fracture morphology represents a typical aspect of brittle fracture mode, consisting of a large amount of cleavage and quasi-cleavage planes, and the presence of micro-cracks.

Using the formalism proposed by the Hall-Petch model, an experimental equation correlating the ultimate tensile strength (UTS) as a function of the equivalent diameter (De) was obtained (Fig. 8), which can permit insights into the pre-programming of material conditions in terms of microstructures, rheocasting

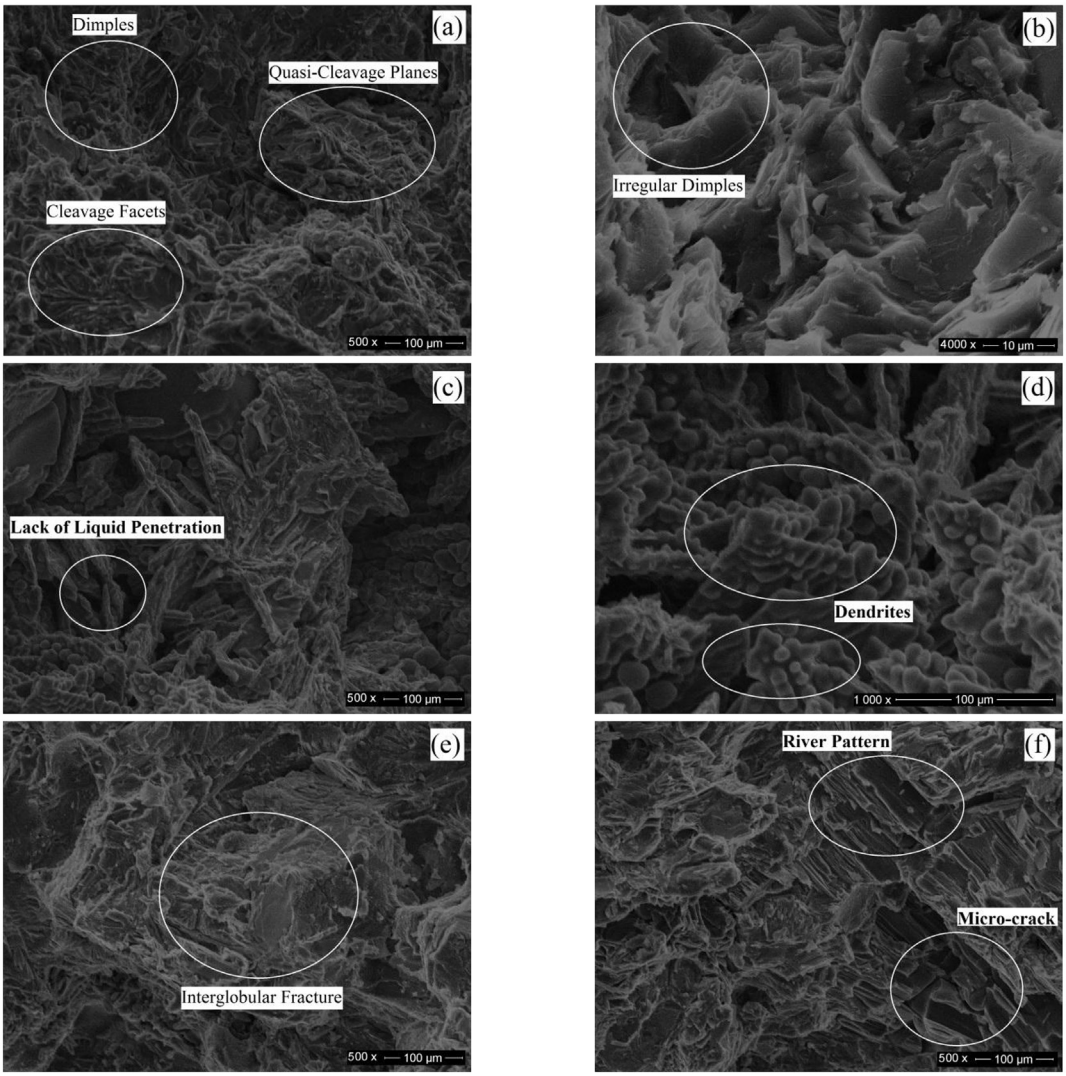

Fig. 7. SEM images of the surface fractures of the tensile test samples in the rheocasting and rapid cooling casting conditions (conventional cast). (a) and (b): Experiment 2: fs = 0.30, 605 °C rheocasting. (c) and (d): Experiment 4: fs = 0.61, 585 °C rheocasting. (e) Experiment 4: fs = 0.49, 595 °C rheocasting. (f) Experiment 5: rapid cooling casting – non-stirrer.

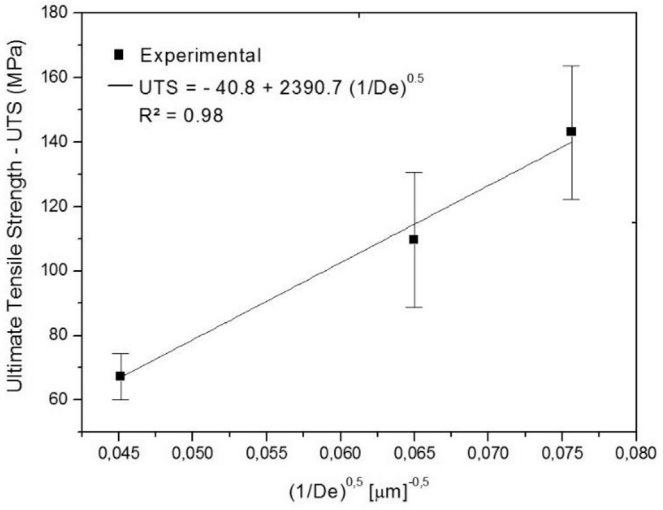

Fig. 8. Ultimate tensile strength (UTS) as a function of equivalent diameter (De).

conditions and desired mechanical properties. As can be observed, a linear behavior between ultimate tensile strength and the size of globules was achieved, and the best results were obtained with lower solid fraction.

4. Conclusions

Based on the results obtained, the following major conclusions can be drawn:

- The thermal analysis applying the CA-CCTA and DSC methods indicated a melting range of 103 °C, which is suitable for rheocasting process.
- Phases formation during solidification are given by: α-Mg matrix (615 °C), $Al_{11}La_3$ acicular phase (605 °C), α-Mg + $(Mg,Al)_2Ca$ refined eutectic (526 °C) and α-Mg + Mg_2Ca coarse eutectic (512 °C).
- For the fs = 0.30 the rheocast showed the presence of $Al_{11}La_3$ only at the globule boundaries, while for fs = 0.49 and fs = 0.61 the $Al_{11}La_3$ is also present inside the globules.
- The highest tensile strength and deformation were observed for fs = 0.30, showing an increase of 77% for ultimate tensile strength and 80% for strain to fracture when compared to the rapid cooling cast without stirring.
- In the fracture surface, the fs = 0.3 presented a mixture ductile-brittle fracture mode, with the presence of quasi-cleavage and dimples. When solid fraction increased to fs = 0.49 and 0.61, the fracture mode showed a transition from ductile-brittle to a fully brittle mode.
- The rheocast samples with fs = 0.49 showed intergranular and transgranular crack propagation modes, while in the rheocast processed with fs = 0.61 the crack propagation was exclusively in the regions of the lack of liquid penetration.

Acknowledgement

The authors acknowledge financial support provided by CAPES and CNPq (The Brazilian Research Council) and FAPERGS (The Scientific Research Foundation of the State of Rio Grande do Sul).

References

[1] W. Zhang, W. Xiao, F. Wang, C. Ma, Development of heat resistant Mg-Zn-Al-based magnesium alloys by addition of La and Ca : microstructure and tensile properties, J. Alloys Compd. 684 (2016) 8–14, https://doi.org/10.1016/j.jallcom.2016.05.137.
[2] Z.Y. Zhao, R.G. Guan, X. Wang, Y. Li, L. Dong, C.S. Lee, C.M. Liu, Microstructure formation mechanism and properties of AZ61 alloy processed by melt treatment with vibrating cooling slope and semisolid rolling, Met. Mater. Int. 19 (2013) 1063–1067, https://doi.org/10.1007/s12540-013-5022-2.
[3] Z. Yang, J.P. Li, J.X. Zhang, G.W. Lorimer, J. Robson, Review on research and development of magnesium alloys, Acta Metall. Sin. (English Lett.) 21 (2008) 313–328, https://doi.org/10.1016/S1006-7191(08)60054-X.
[4] E. Ayman, U. Junko, K. Katsuyoshi, Application of rapid solidification powder metallurgy to the fabrication of high-strength , high-ductility Mg–Al–Zn–Ca–La alloy through hot extrusion, Acta Mater. 59 (2011) 273–282, https://doi.org/10.1016/j.actamat.2010.09.031.
[5] A. Suzuki, N.D. Saddock, J.W. Jones, T.M. Pollock, Solidification paths and eutectic intermetallic phases in Mg–Al–Ca ternary alloys, Acta Mater. 53 (2005) 2823–2834, https://doi.org/10.1016/j.actamat.2005.03.001.
[6] X. Fang, S. Lü, L. Zhao, J. Wang, L. Liu, S. Wu, Microstructure and mechanical properties of a novel Mg–RE–Zn–Y alloy fabricated by rheo-squeeze casting, Mater. Des. 94 (2016) 353–359, https://doi.org/10.1016/j.matdes.2016.01.063.
[7] B. Kondori, R. Mahmudi, Effect of Ca additions on the microstructure and creep properties of a cast Mg–Al–Mn magnesium alloy, Mater. Sci. Eng. A 700 (2017) 438–447, https://doi.org/10.1016/j.msea.2017.06.007.
[8] C. Wang, A. Chen, L. Zhang, W. Liu, G. Wu, W. Ding, Preparation of an Mg–Gd–Zn alloy semisolid slurry by low frequency electro-magnetic stirring, Mater. Des. 84 (2015) 53–63, https://doi.org/10.1016/j.matdes.2015.06.126.
[9] R. Canyook, J. Wannasin, S. Wisuthmethangkul, M.C. Flemings, Characterization of the microstructure evolution of a semisolid metal slurry during the early stages, Acta Mater. 60 (2012) 3501–3510, https://doi.org/10.1016/j.actamat.2012.03.002.
[10] R. Canyook, S. Petsut, S. Wisutmethangoon, M.C. Flemings, J. Wannasin, Evolution of microstructure in semisolid slurries of Rheocast aluminum alloy, Trans. Nonferrous Metals Soc. China 20 (2010) 1649–1655, https://doi.org/10.1016/S1003-6326(09)60353-8.
[11] H. Chen, J. Chen, J. Liao, The influence of shearing conditions on the rheology of semisolid magnesium alloy, Mater. Sci. Eng. A 487 (2008) 114–119, https://doi.org/10.1016/j.msea.2007.09.072.
[12] Q. Chen, G. Chen, L. Han, N. Hu, F. Han, Z. Zhao, X. Xia, Y. Wan, Microstructure evolution of SiCp/ZM6 (Mg-Nd-Zn) magnesium matrix composite in the semisolid state, J. Alloys Compd. 656 (2016) 67–76, https://doi.org/10.1016/j.jallcom.2015.09.135.
[13] Z. Fan, Semisolid metal processing, Int. Mater. Rev. 47 (2) (2002) 49–85, https://doi.org/10.1179/095066001225001076.
[14] B. Zhou, Y. Kang, G. Zhu, J. Gao, M. Qi, H. Zhang, Forced convection rheoforming process for preparation of 7075 aluminum alloy semisolid slurry and its numerical simulation, Trans. Nonferrous Metals Soc. China 24 (2014) 1109–1116, https://doi.org/10.1016/S1003-6326(14)63169-1.
[15] Y. Zhang, G. Wu, W. Liu, L. Zhang, S. Pang, W. Ding, Microstructure and mechanical properties of rheo-squeeze casting AZ91-Ca magnesium alloy prepared by gas bubbling process, J. Mater. 67 (2015) 1–8, https://doi.org/10.1016/j.matdes.2014.10.087.
[16] H. Wenxian, Y.A.N. Hong, Preparation and theoretic study of semisolid Al 2 Y/AZ91 magnesium matrix composites slurry by ultrasonic vibration, J. Rare Earths 32 (2014) 573–579, https://doi.org/10.1016/S1002-0721(14)60110-1.
[17] Q. Chen, G. Chen, L. Han, N. Hu, F. Han, Z. Zhao, X. Xia, Y. Wan, Microstructure evolution of SiCp/ZM6 (Mg-Nd-Zn) magnesium matrix composite in the semisolid state, J. Alloys Compd. 656 (2016) 67–76, https://doi.org/10.1016/j.jallcom.2015.09.135.
[18] C.D. Yim, K.S. Shin, Changes in microstructure and hardness of rheocast AZ91HP magnesium alloy with stirring conditions, Mater. Sci. Eng. A 395 (2005) 226–232, https://doi.org/10.1016/j.msea.2004.12.050.
[19] M.E. Farina, P. Bell, C.R.F. Ferreira, B.A. Dedavid, Effects of solidification rate in the microstructure of Al-Si5Cu3 aluminum cast alloy, Mater. Res. 20 (2017) 273–278, https://doi.org/10.1590/1980-5373-MR-2017-0083.
[20] ASTM-B557, Standard Test Methods of Tension Testing Wrought and Cast Aluminum and Magnesium-alloy Products, ASTM, 2003.
[21] T.V. Ferri, A.P. Figueiredo, C.R.F. Ferreira, W. Hormaza, C.A. Santos, J.A. Spim, Mechanical properties as a function of microstructure in the new Mg-Al-Ca-La alloy solidified under different conditions, Mater. Sci. Eng. A 527 (2010) 4624–4632, https://doi.org/10.1016/j.msea.2010.03.041.
[22] S.M. Liang, R.S. Chen, J.J. Blandin, M. Suery, E.H. Han, Thermal analysis and solidification pathways of Mg-Al-Ca system alloys, Mater. Sci. Eng. A 480 (2008) 365–372, https://doi.org/10.1016/j.msea.2007.07.025.
[23] L. Han, H. Hu, D.O. Northwood, N. Li, Microstructure and nano-scale mechanical behavior of Mg-Al and Mg-Al-Ca alloys, Mater. Sci. Eng. A 473 (2008) 16–27, https://doi.org/10.1016/j.msea.2007.073.053.
[24] Y. Liu, N. Wang, J. Wang, B. Ma, D. Zhao, Investigation of the crystallographic structure and orientations of the Al2Ca phase in a Mg-Al-Ca-Mn alloy, Mater. Char. 142 (2018) 377–382, https://doi.org/10.1016/j.matchar.2018.05.047.
[25] L. Zhang, K-k. Deng, K-b. Nie, F-j. Xu, K. Su, W. Liang, Microstructures and mechanical properties of Mg-Al-Ca alloys affected by Ca/Al ratio, Mater. Sci. Eng. A 636 (2015) 279–288, https://doi.org/10.1016/j.msea.2015.03.100.
[26] H.I. Chen, J.C. Chen, J.J. Liao, The influence of shearing conditions on the rheology of semisolid magnesium alloy, Mater. Sci. Eng. A 487 (2008)

114–119, https://doi.org/10.1016/j.msea.2007.09.072.
[27] M. Li, Y. Li, H. Zheng, X. Huang, T. Chen, Y. Ma, Solidification behavior of 6061 wrought aluminum alloy during rheo-diecasting process with self-inoculation method, Trans. Nonferrous Metals Soc. China 28 (2018) 879–889, https://doi.org/10.1016/S1003-6326(18)64721-1.
[28] E.P. Silva, F. Marques, T.S. Nossa, U. Alfaro, H.C. Pinto, Impact of Ce-base mischmetal on the microstructure and mechanical behavior of ZK60 magnesium casting alloys, Mater. Sci. Eng. A 723 (2018) 306–313, https://doi.org/10.1016/j.msea.2018.02.024.
[29] S. Lü, S. Wu, Z. Zhu, P. An, Effect of semisolid processing on microstructure and mechanical properties of 5052 aluminum alloy, Trans. Nonferrous Metals Soc. China 20 (2010) 758–762.
[30] Q. Tang, M. Zhou, L. Fan, Y. Zhang, G. Quan, B. Liu, Constitutive behaviour of AZ80 magnesium alloy compressed at elevated temperature and containing a small fraction of liquid, Vacuun 155 (2018) 476–489, https://doi.org/10.1016/j.vacuum.2018.06.053.
[31] C. Chu, Z. Hu, X. Li, H. Yan, X. Wu, Y. Mai, Evolution and distribution of Al 2 Sm phase in as-extruded AZ61 – x Sm magnesium alloys during semi-solid isothermal heat-treatment, Trans. Nonferrous Metals Soc. China 28 (2018) 1311–1320, https://doi.org/10.1016/S1003-6326(18)64768-5.
[32] M.C. Flemings, R.G. Riek, K.P. Yang, Rheocasting, Mater. Sci. Eng. 25 (1976) 103–117.
[33] H.V. Atkinson, Modelling the semisolid processing of metallic alloys, Prog. Mater. Sci. 50 (2005) 341–412, https://doi.org/10.1016/j.pmatsci.2004.04.003.